Measuring Porosity in Ti-6Al-4V Laser Powder Bed Fusion Samples

Wei-Ling (Winnie) Hung
Faculty Advisor: Dr. Jerard V. Gordon
Department of Mechanical Engineering, University of Michigan

Abstract

Accurate characterization and prediction of porosity defects in laser powder bed fusion (LPBF) has great potential in improving the structural integrity and durability of the additive manufactured metallic parts. In previous research by Dr. Jerard Gordon, a predictive model for lack of fusion (LOF) and keyhole defect formation in Ti-6Al-4V LPBF parts under different printing laser power and speed was developed. This project builds upon Dr. Gordon's research and aims to validate the model by printing 16 samples in the TRUMPF TruPrint 1000 under different laser settings ranging from 60 W to 120 W in power and 0.1 to 0.75 m/s in velocity. The experimentally obtained porosities show a positive correlation with the predicted lack of fusion criteria despite not being a strong linear relationship. Overall, this study shows how changing the LPBF printing parameters can affect porosity formation in printed parts.

Keywords: metal additive manufacturing, laser powder bed fusion, Ti-6Al-4V, lack of fusion, keyholing, porosity defect

I. Introduction

Metal additive manufacturing (metal AM), or metal 3D printing, is a promising manufacturing process that allows for unprecedented design freedom and eliminates the need for custom tools compared to traditional methods of metal manufacturing. Laser powder bed fusion (LPBF) is one of the most popular forms of metal AM that produces parts by melting and fusing metal powder layer by layer on a platform using a focused laser beam. The choice of Ti-6Al-4V, or Ti64, comes from the alloy's good mechanical properties, exceptional corrosion resistance, and outstanding biocompatibility, all of which making it the most commonly used titanium alloy [1].

While the notable material properties of Ti-6Al-4V gave it far-reaching potentials in the aerospace, automotive, biomechanical, chemical, and other industries, conventional ways of manufacturing have limited its application. As LPBF matured as an advanced metal AM technology, its ability to produce complex geometries at high resolutions has attracted much attention in both academia and industry [2]. Despite being relatively well-researched, LPBF porosity defects have yet to be completely understood, and such undesired defects are deleterious to the structural integrity and durability of the additive manufactured parts, often contributing to their premature failures (e.g., fatigue) [3].

Understanding and predicting porosity defect formation, more specifically lack of fusion porosity formation, is therefore the ultimate goal of this research.

Laser Powder Bed Fusion (LPBF)

Laser powder bed fusion (LPBF), also known as selective laser melting (SLM) or direct metal laser melting (DMLM) [1], is a metal additive process that employs a laser beam to fabricate the part layer by layer. A simplified schematic diagram of a LPBF printer is shown in Figure 1. The build process starts from the roller spreading a layer of metallic powder of specified thickness (defined as the layer thickness L) onto the powder bed. The laser then focuses on the cross-sectional area of the CAD model to melt and fuse the powder. After the melt pool is cooled and solidified, the build plate is moved down by a distance L to allow the process to start over again. These steps are repeated until the entire part is built.

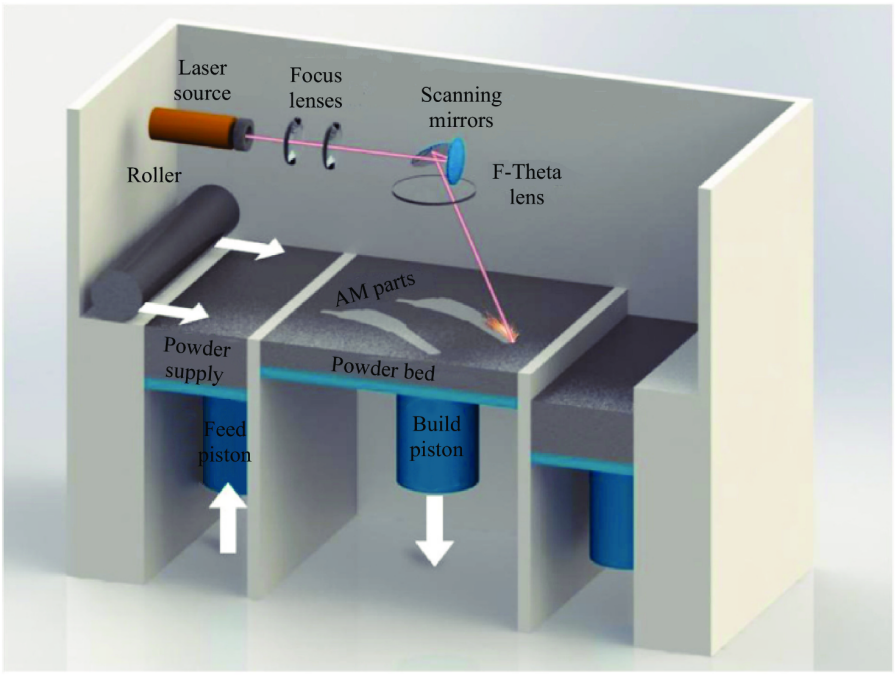

Figure 1: Schematic diagram showing the mechanism of a common LPBF machine [1].

Common Defects in Metal AM

Four types of common defects in LPBF are lack of fusion (LOF) porosity, keyhole porosity, balling, and solidification cracking [2][3]. Balling is a surface defect where the combination of surface tension and capillary forces drive the liquid phase in the molten pool into a sphere, which has a lower surface energy [4]; solidification cracking is the

fracture of the thin layer of the melt pool at the dendrite grain boundaries during rapid cooling [2].

While both balling and hot cracks are important metallurgical defects in LPBF processes, the focus of this research is on porosity formation, especially LOF porosities. LOF results in larger pore sizes compared to keyholing, and thus it has a greater impact on the structural integrity of the printed parts. LOF porosities are formed when adjacent melt pool tracks, as shown in Figure 2 below, have insufficient overlap, resulting in volumes in the printed geometry not being fused [5]. In other words, to avoid LOF pore formation, every point must be melted at least once [3].

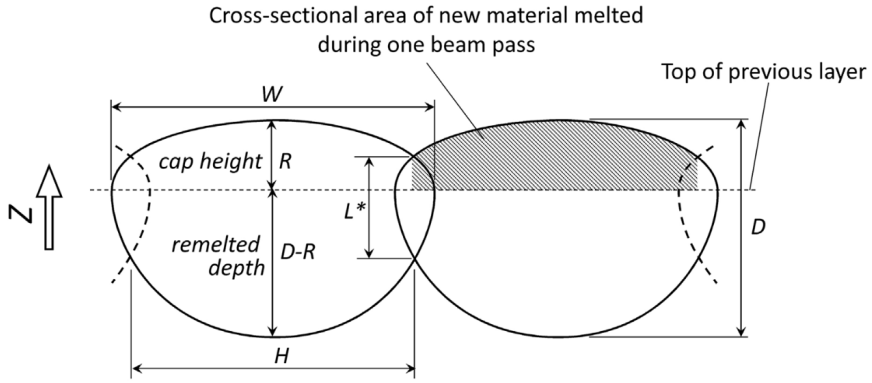

Figure 2: Assuming a dual half-elliptical melt pool shape, the illustration shows the overlap between two adjacent melt pool tracks when the build direction is in the labeled z-direction [5]. Some important dimensions are also labeled in the figure.

In contrast to LOF porosity, keyhole pore formation corresponds to vapor bubbles trapped in deep keyholes [3]. These defects are usually much smaller than LOF pores.

Prediction of LOF Pores

The underlying principle for complete melting of all points is that the depth of the overlapping area of two adjacent melt pools, L^*, as labeled in Figure 2 above, must be greater than or equal to the layer thickness L (e.g., $L^* \geq L$). When this is satisfied, LOF porosity is not expected to form [5]. Through calculations done by Tang, Pistorius, and Beuth, the relationship $L^* \geq L$ is can be expressed in the form of Equation 1:

$$\left(\frac{H}{W}\right)^2 + \left(\frac{L}{D}\right)^2 \leq 1 \qquad (1)[5]$$

where H is the hatch spacing, W is the melt pool width, and D is the total melt pool depth. H, W, and D are as labeled in Figure 2 and L is a printing parameter.

The total melt pool depth, D, is estimated using the Rosenthal Equation, which accounts for the material parameters. Assuming a dual half-elliptical cross-sectional shape of the melt pool with center to center distance equal to H, D can be calculated using Equation 2 below:

$$D = \sqrt{\frac{2Q\varepsilon}{\pi e \rho C_p V (T_{melt} - T_0)}} \quad (2)[3]$$

where Q is the laser power in W, ε is the absorptivity, e is the natural exponent, ρ is the density in kg/m^3, Cp is the specific heat capacity in J/kg · K, V is the laser scan velocity in m/s, T_{melt} is the melting temperature in K, and T_0 is the initial temperature also in K [3].

Defect Structure Process Mapping

Based on Equations 2 and 3, Dr. Gordon developed a model predicting the boundaries for LOF and keyhole defect formation in his research, known as the defect structure process map (DSPM) and shown below in Figure 3.

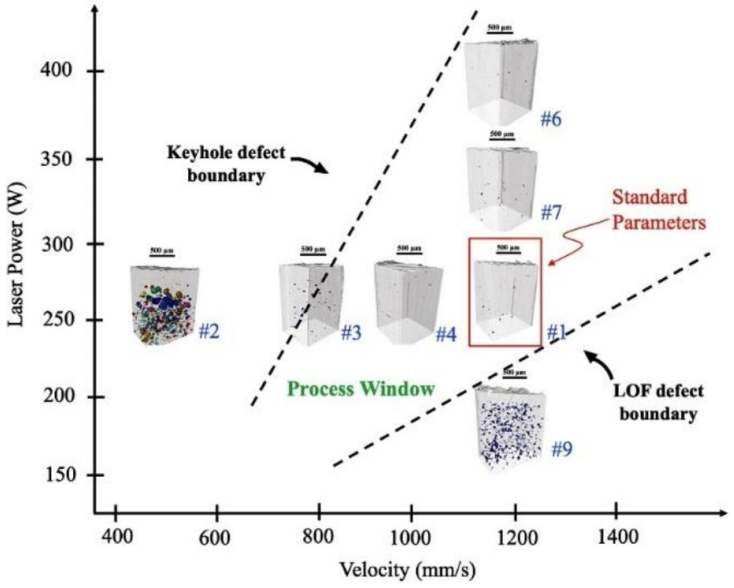

Figure 3: The defect structure process map (DSPM) developed by Dr. Gordon [3].

The DSPM predicts that below the LOF defect boundary, at high laser velocity and low power, LOF porosities will form; on the other hand, above the keyhole defect boundary,

when printing at low velocity and high laser power, keyhole porosities are expected to form.

II. Methods

To validate the DSPM, LPBF samples are printed, post-processed, imaged under an optical microscope, and analyzed using ImageJ.

Sample Printing and Post-Processing

Based on the DSPM, 16 cubic samples of 1 cm^3 were printed under different combinations of laser power and speed on the TRUMPF TruPrint 1000. The printing parameters used for each sample are listed in Table 1 on pages 7 and 8.

After being printed, the samples were cut off the base plate using wire EDM and further cut in half using a vertical band saw approximately halfway between the top and bottom surfaces. This allows us to perform light optical microscopy on a cross-section instead of on the surface.

To prepare the samples for light optical microscopy, the samples were mounted in pucks using the sample mounting press in the Van Vlack Laboratory. They then went through a series of grinding and polishing processes using in order grit P400 sandpaper, grit P600 sandpaper, grit P800 sandpaper, grit P1200 sandpaper, grit P2500 sandpaper, and finally 1 μm diamond solution. Figure 4 below shows the samples after the final polishing.

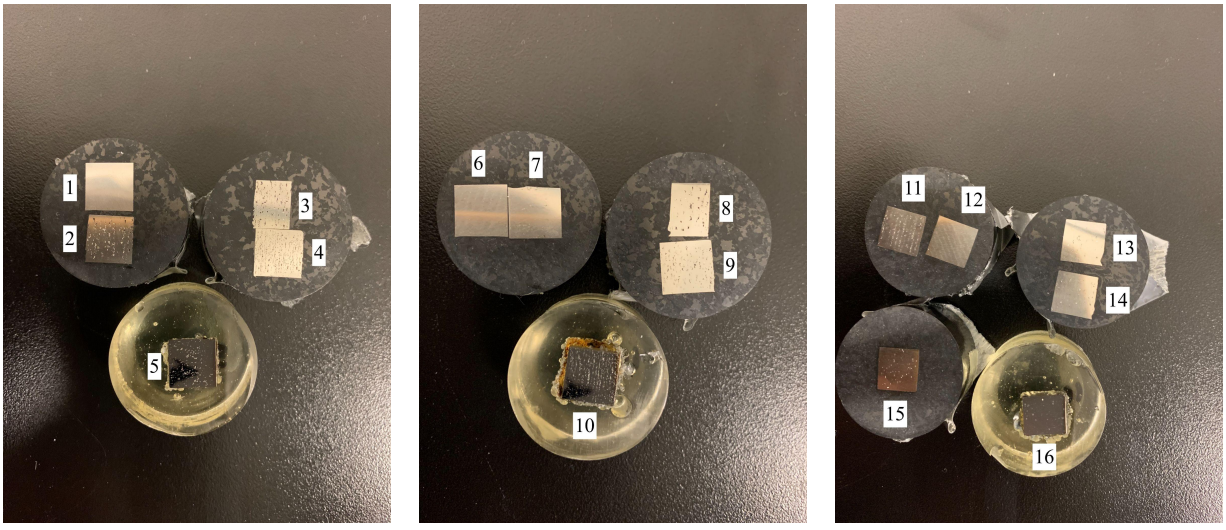

Figure 4: The 16 samples after they've been printed, mounted, and grinded/polished. Some samples are mounted in the same puck for efficiency.

Light Optical Microscopy and ImageJ

With the samples ready for light optical microscopy, they were observed and imaged under a Nikon Optiphot microscope in Dr. Amit Misra's lab. Three areas were randomly chosen on each sample and viewed under 5X, 10X, 40X, and 100X magnification in order.

Although four different magnifications were used to observe the samples, it was decided that the 5X magnification was the most ideal. Therefore, importing the 5X images of each sample into ImageJ, we were able to calculate the the porosity (%) using areas selected:

$$Porosity = (1 - \frac{Solid\ area}{Total\ area}) \times 100\% \quad (3)$$

where *Solid area* is the area with fused Ti-6Al-4V material, and *Total area* is the total area of the sample that can be seen through the window under 5X magnification.

III. Optical Microscopy Results

All 16 samples were imaged under 5X magnification and their porosities are calculated in ImageJ. LOF pores and keyholing pores are easily distinguishable in the light optical images taken: LOF pores are large and irregular in shape; in contrast, keyholing pores are smaller and round since they are a result of trapped gas bubbles. The differences can be observed in two representative samples, Figures 5 (sample 4, where LOF is expected to form) and 6 (sample 4, where LOF is not expected to form) below. The rest of the sample images can be found in Table A in the appendix.

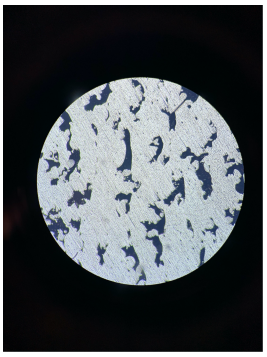

(a)

(b)

Figure 5: Optical image of sample 4 (a) and its ImageJ processed result (b). This sample has mainly LOF pores and its porosity is calculated to be 13.731%.

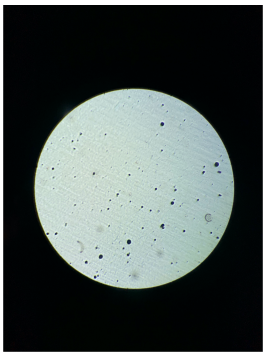

(a)

(b)

Figure 6: Optical image of sample 16 (a) and its ImageJ processed result (b). Only keyhole defects are observed in this sample and its porosity is 2.131%.

IV. Sample Analysis and Discussion

The porosity results for the 16 Ti-6Al-4V LPBF samples are summarized in Table 1 below. A linear regression line was plotted between the LOF criteria (predicted results) and the measured porosity (experimental results). The R^2 value for the linear fit is 0.575. Experimental results generally follow a trend consistent with the model except for sample 11. Sample 11 is observed to have LOF defects despite being printed at high power and low velocity, which gives it a low LOF criteria value. The cause of this deviation from the DSPM is unclear.

Table 1: The printing parameters, LOF criteria for prediction, and measured porosity of each of the 16 samples.

Sample	Power (W)	Velocity (m/s)	LOF Criteria	Porosity	LOF?
1	60	0.1	0.10010697	0.456%	
2	60	0.3	0.30032092	9.112%	x
3	60	0.5	0.50053486	12.061%	x
4	60	0.75	0.70074881	13.731%	x
5	60	1	0.90096275	13.763%	x
6	90	0.1	0.06673798	0.385%	
7	90	0.3	0.20021394	1.22%	x
8	90	0.5	0.33368991	7.079%	x
9	90	0.75	0.46716587	5.876%	x
10	90	1	0.60064183	15.636%	x
11	120	0.1	0.05005349	8.95%	x
12	120	0.3	0.15016046	0.899%	
13	120	0.5	0.25026743	5.992%	x
14	120	0.75	0.3503744	5.969%	x
15	120	1	0.45048138	2.993%	x
16	80	0.2	Nominal	2.131%	

In conclusion, a positive correlation is observed between the predicted LOF criteria and the experimentally measured porosity in the 16 samples, although the linear relationship is not strong. With these results and further research in the future, the DSPM can become an important cornerstone for understanding and predicting LOF porosity defect formation in LPBF Ti-6Al-4V part fabrication, therefore expanding the potential of LPBF overall.

V. Acknowledgements

This project would not have been possible without the guidance and previous research done by Dr. Jerard Gordon. It also would not have been possible without the support of Michael Stryk, Audrey Yung, and Daniel Rubio-Ejchel. Finally, my appreciation goes to Dr. Amit Misra's lab for letting me use their microscope.

VI. References

[1] Cao, Sheng, et al. "Review of Laser Powder Bed Fusion (LPBF) Fabricated Ti-6Al-4V: Process, Post-Process Treatment, Microstructure, and Property." *Light: Advanced Manufacturing,* vol. 2, Issue 3, 2021. http://dx.doi.org/10.37188/lam.2021.020.

[2] Qin, Siyuan, et al. "Influence of Process Parameters on Porosity and Hot Cracking of AISI H13 Fabricated by Laser Powder Bed Fusion." *Powders,* 2022. https://doi.org/10.3390/powders1030012.

[3] Gordon, Jerard, et al. "Defect Structures Process Maps for Laser Powder Bed Fusion Additive Manufacturing." *Additive Manufacturing,* vol. 36, 2022. https://doi.org/10.1016/j.addma.2020.101552.

[4] Narasimharaju, Shubhavardhan Ramadurga, et al. "A Comprehensive Review on Laser Powder Bed Fusion of Steels: Processing, Microstructure, Defects and Control Methods, Mechanical Properties, Current Challenges and Future Trends." *Journal of Manufacturing Processes,* vol. 75, 2022, pp 375-414. https://doi.org/10.1016/j.jmapro.2021.12.033.

[5] Tang, Ming, et al. "Prediction of Lack-of-Fusion Porosity for Powder Bed Fusion." *Additive Manufacturing,* vol. 14, 2017, pp. 39-48. http://dx.doi.org/10.1016/j.addma.2016.12.001.

VII. Appendix

Table A: Optical images (left) of each of the 16 samples with their ImageJ-processed images (right). All of the images were taken under 5X magnification, with the diameter of the circular window being 3800 μm. LOF pores and keyholing pores are easily distinguishable in these images as LOF pores are large and irregular in shape, while keyholing pores are smaller and round.

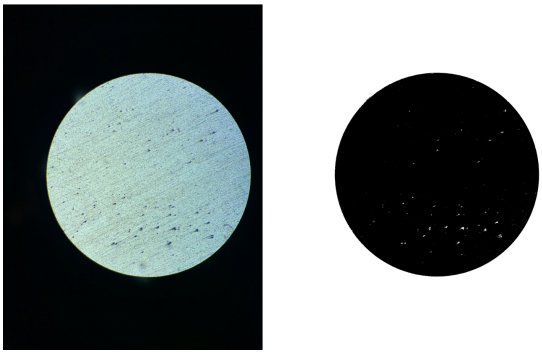 Sample 1: calculated porosity of 0.46% and no LOF observed	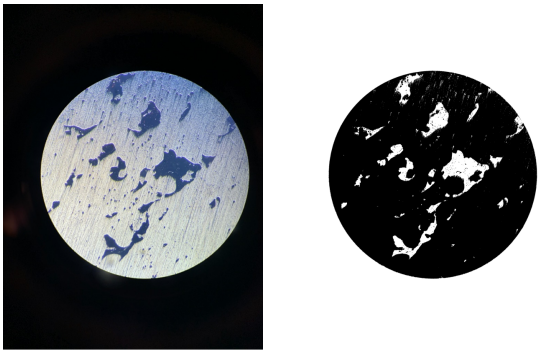 Sample 2: calculated porosity of 9.11% and LOF is observed
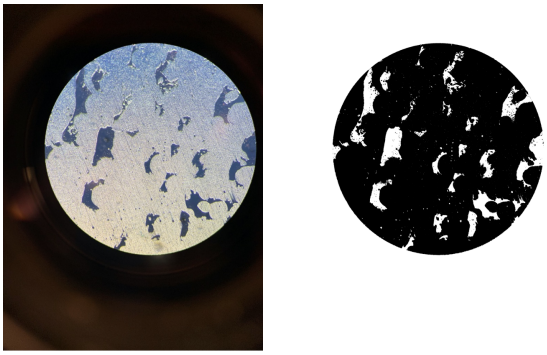 Sample 3: calculated porosity of 12.06% and LOF is observed	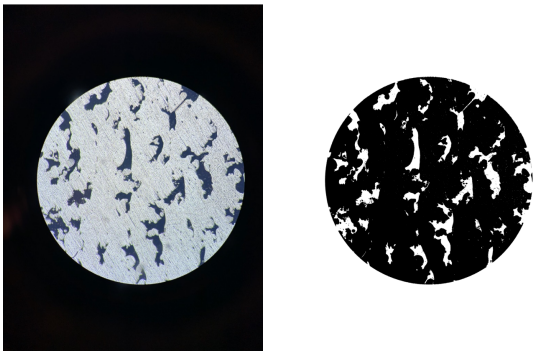 Sample 4: calculated porosity of 13.73% and LOF is observed
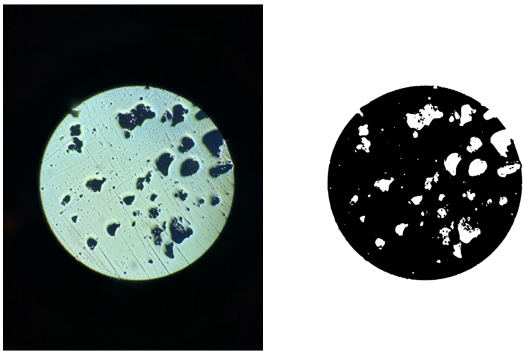 Sample 5: calculated porosity of 13.76% and LOF is observed	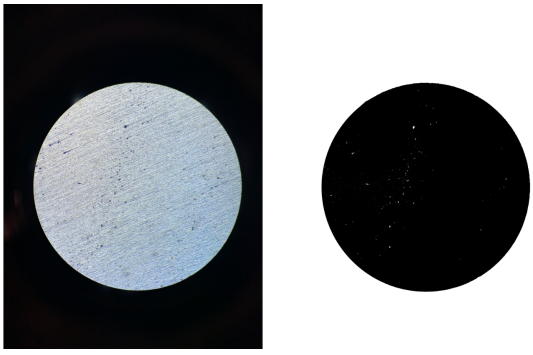 Sample 6: calculated porosity of 0.39% and no LOF observed

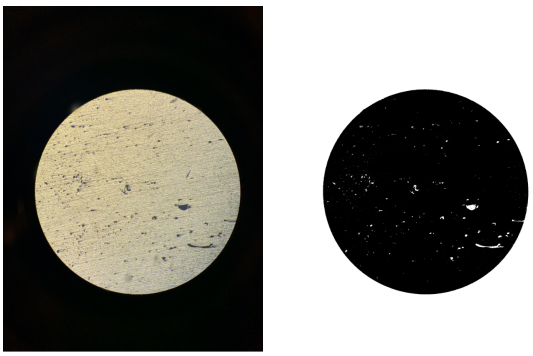 Sample 7: calculated porosity of 1.22% and LOF is observed	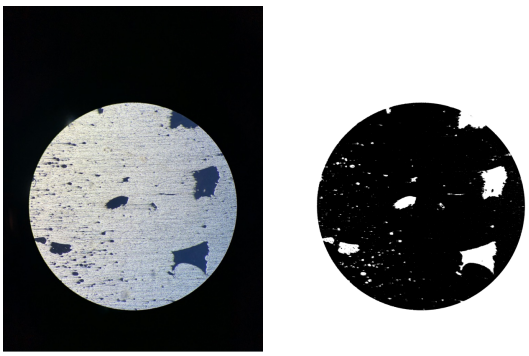 Sample 8: calculated porosity of 7.08% and LOF is observed
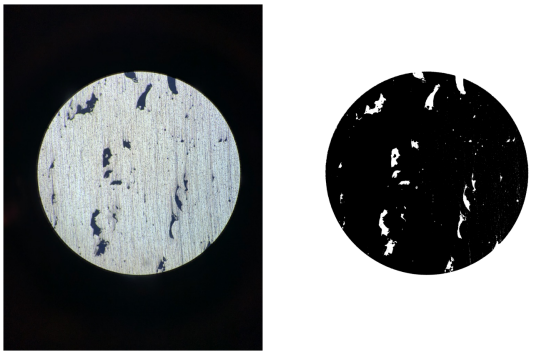 Sample 9: calculated porosity of 5.88% and LOF is observed	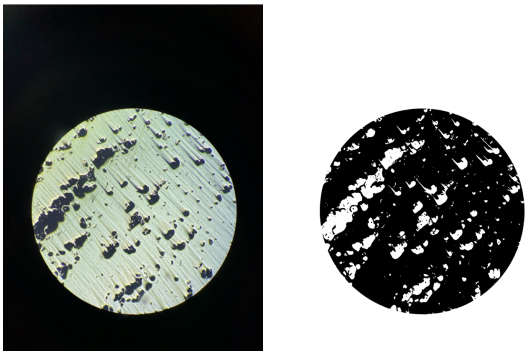 Sample 10: calculated porosity of 15.64% and LOF is observed
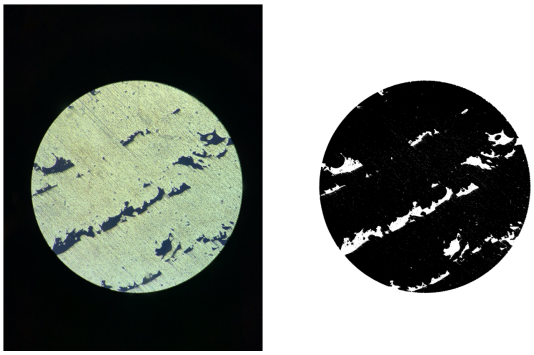 Sample 11: calculated porosity of 8.95% and LOF is observed	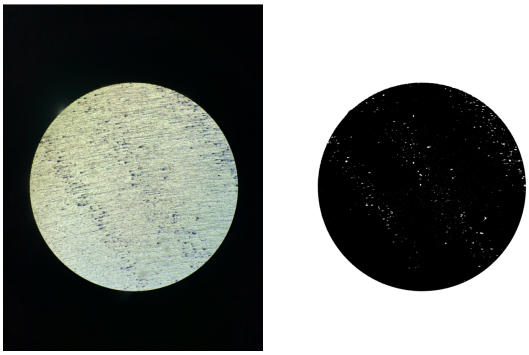 Sample 12: calculated porosity of 0.90% and no LOF observed

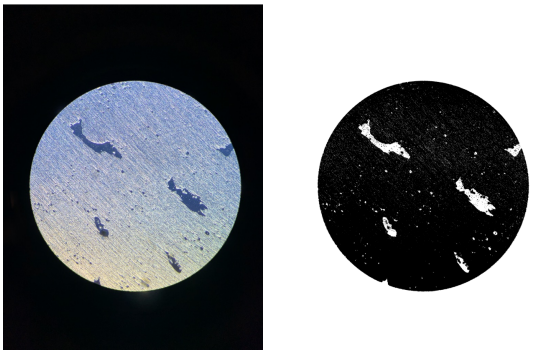 Sample 13: calculated porosity of 5.99% and LOF is observed	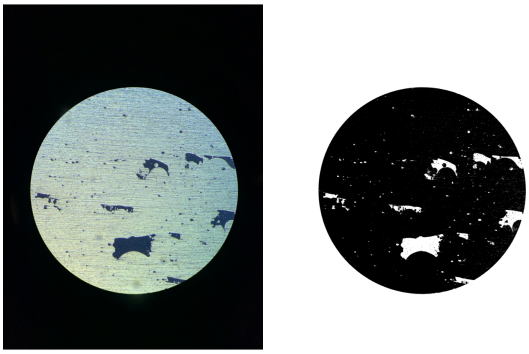 Sample 14: calculated porosity of 5.97% and LOF is observed
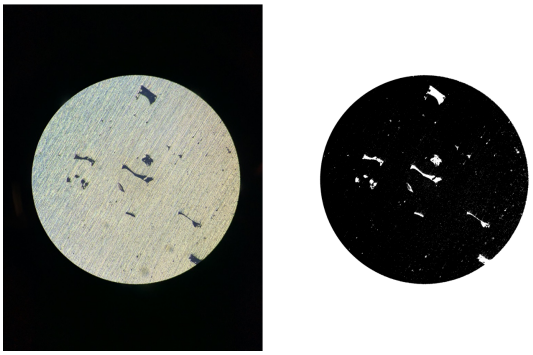 Sample 15: calculated porosity of 2.99% and LOF is observed	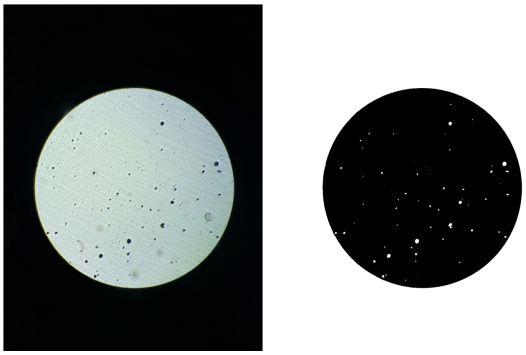 Sample 16: calculated porosity of 2.13% and no LOF observed